Sensors and Materials, Vol. 38, No. 6 (2026) 3133–3142
MYU Tokyo

S & M 4493

Laser Sintering of Ceramic Coatings on 304 Stainless Steel: Effects of Energy Input on Microstructure, Hardness, and Wear

Shih-Chen Shi,* Po-Chun Wang, and Guan-Yu Chen

Department of Mechanical Engineering, National Cheng Kung University (NCKU),
No. 1, University Road, Tainan 70101, Taiwan

(Received January 14, 2026; accepted May 15, 2026)

Keywords: laser sintering, ceramic coatings, Vickers hardness, wear behavior

Laser sintering has emerged as an effective technique for fabricating ceramic coatings with localized energy input and rapid processing capability. In this study, Al_2O_3, 8 mol% yttria-stabilized zirconia (8-YSZ), and silicon carbide (SiC) ceramic coatings were fabricated on 304 stainless steel substrates via laser sintering. The effects of laser energy input on the coating microstructure, phase stability, mechanical hardness, and wear behavior were systematically investigated. X-ray diffraction analysis confirmed that all coatings retained their primary crystalline phases after laser sintering, indicating that rapid heating and cooling suppressed undesirable phase transformation. Optical and scanning electron microscopy observations revealed that appropriate laser power promoted uniform melting, reduced porosity, and improved coating continuity. In contrast, insufficient or excessive energy input led to incomplete sintering or localized overmelting. Vickers hardness measurements showed that coating hardness increased with densification, reaching maximum values of approximately 2780 N/mm² for Al_2O_3 and 8-YSZ, and 7560 N/mm² for SiC under optimal laser conditions. Wear tests demonstrated that laser-sintered ceramic coatings showed significantly enhanced tribological performance compared with the uncoated stainless steel substrate, with SiC exhibiting the lowest friction coefficient and the highest wear resistance. These results demonstrate that the precise control of laser energy input is critical for optimizing coating performance and highlights laser sintering as a promising approach for producing high-performance ceramic coatings for high-wear applications.

1. Introduction

With the advancement of manufacturing and energy conversion technologies, the stability and reliability of materials under extreme environments have become critical.[1–3] Type 304 stainless steel is widely applied in structural and energy-related fields owing to its good mechanical strength and corrosion resistance.[4,5] However, high-temperature oxidation and thermal cycling often cause surface degradation and mechanical deterioration, limiting its high-temperature applicability.[6,7] Specifically, in the semiconductor industry, the materials used in

*Corresponding author: e-mail: scshi@mail.ncku.edu.tw
https://doi.org/10.18494/SAM6173

ISSN 0914-4935
https://myukk.org/

wafer processing equipment must withstand increasingly harsh environments, including corrosive plasma erosion and mechanical wear.[8] Ceramic coatings, particularly alumina (Al_2O_3), 8 mol% yttria-stabilized zirconia (8-YSZ), and silicon carbide (SiC), have emerged as critical solutions for components such as electrostatic chucks, focus rings, and gas distribution plates. These coatings provide superior dielectric properties and exceptional resistance to plasma etching, which are essential for maintaining contamination-free performance in advanced manufacturing.[9,10]

In the field of metal-based composite coatings, laser processing technologies have increasingly superseded conventional sintering and deposition methods.[11,12] These processes provide high energy density, rapid thermal cycles, and precise localized control, enabling superior microstructural characteristics compared with furnace sintering. In this study, a clear distinction is made between two primary mechanisms: laser sintering, which involves the partial melting and consolidation of ceramic powders through localized heat-induced particle bridging, and laser cladding, which typically entails the complete melting of the feed material to produce thicker deposits and achieve a robust metallurgical bond with the metallic substrate. Consequently, laser-based processing significantly shortens production time, minimizes the heat-affected zone (HAZ), and enhances coating densification.[13,14]

Al_2O_3, 8-YSZ, and SiC are commonly used ceramic coating materials. Al_2O_3 offers high hardness and chemical stability,[15–17] but it exhibits a thermal expansion mismatch with metals. 8-YSZ features low thermal conductivity and good phase stability,[18] making it suitable for thermal barrier coatings, while SiC provides high thermal conductivity and excellent wear resistance at elevated temperatures.[19] Differences in interfacial behavior and thermal stress significantly affect coating performance.

Previous studies have revealed that laser power, scanning speed, and defocusing distance strongly affect coating thickness and densification.[20,21] Appropriate laser energy promotes dense coatings, whereas excessive energy induces pores and cracks, highlighting the critical interaction between laser parameters and ceramic properties.[22,23] However, most studies have been focused on single ceramic systems or laser parameter optimization. Comparative evaluations of Al_2O_3, 8-YSZ, and SiC under identical laser conditions, integrating microstructure, hardness, and wear behavior, remain limited.

Therefore, in this study, we deposited Al_2O_3, 8-YSZ, and SiC powders onto 304 stainless steel using identical laser sintering parameters. The rationale for employing a uniform processing strategy is to establish a controlled experimental baseline, enabling a direct comparison of material-dependent behaviors. By maintaining constant external variables, the variations in coating densification and performance can be isolated and specifically attributed to the intrinsic thermophysical and mechanical properties of each ceramic species. X-ray diffraction (XRD), SEM, hardness testing, and wear analysis were subsequently employed to clarify how these material properties and densification affect wear behavior, providing guidance for ceramic-based surface reinforcement in high-wear environments.

2. Materials and Laser Processing

2.1 Materials

Al_2O_3 (15 μm), 8-YSZ (50 μm), and SiC (75 μm) powders were used as coating materials. Commercial 304 stainless steel substrates with a thickness of 0.3 mm were employed.

2.2 Laser sintering procedure

All coatings were fabricated under identical environmental control conditions. Ceramic powders were uniformly deposited onto the substrate surface using a custom-made 0.3 mm stainless steel blade, with the preset powder layer thickness maintained at 0.3 mm. The specimens were fixed in an acrylic fixture and processed in a sealed chamber. Before laser processing, the chamber was evacuated and subsequently backfilled with high-purity argon; the argon pressure was maintained at 12 kPa to suppress oxidation during sintering. The use of a relatively thin (0.3 mm) 304 stainless steel substrate was intentional to facilitate rapid heat dissipation into the underlying fixture, thereby generating steep thermal gradients that affect melt pool stability while effectively suppressing the expansion of the HAZ.

Laser sintering was performed using a wobble-scanning strategy comprising five parallel linear scan paths with 10% overlap to ensure coating continuity. The wobble width and frequency were fixed at 1.5 mm and 193 Hz, respectively. The scanning speed and defocus distance were adjusted for each ceramic material to achieve stable melting behavior. The laser power was systematically varied to evaluate its effects on coating densification and interfacial bonding.

The laser power ranges were 171–207 W for Al_2O_3, 101–155 W for 8-YSZ, and 155–179 W for SiC. In this study, laser energy input was defined as the material-specific power window that facilitates stable melt pool formation and effective densification. The adoption of different power ranges was necessary to compensate the distinct thermophysical characteristics of each ceramic species, specifically the high thermal conductivity of SiC compared with the low thermal conductivity and high phase stability of 8-YSZ. By tailoring the energy input to achieve a comparable level of surface integrity and sintering quality for each system, a consistent baseline was established for evaluating the resulting hardness and wear performance across the three different coatings.

2.3 Characterization and testing

Surface and cross-sectional morphologies were examined by optical microscopy (OM) and SEM. Elemental distribution and phase composition were analyzed by energy-dispersive spectroscopy (EDS), elemental mapping, and XRD. Mechanical properties were evaluated by Vickers hardness testing (9.81 N, 20 s). Surface roughness measurements and three-point bending tests were conducted to assess surface quality and coating–substrate bonding. Electrochemical testing was carried out to evaluate coating porosity, and accelerated wear tests were performed to determine wear resistance.

3. Results and Discussion

3.1 Surface morphology after laser sintering

Surface morphologies of the laser-sintered ceramic coatings were examined by OM and SEM. The results indicate that coating morphology and melting behavior were strongly dependent on laser power. In general, increasing the laser power enhanced powder melting and improved surface continuity.

For Al_2O_3 coatings, moderate laser power (defined here as 171–207 W) produced smooth surfaces with uniform pore distribution and clear melt boundaries, indicating effective densification. At 163 W, insufficient energy prevented the formation of a continuous coating, whereas excessive laser power (above 213 W) led to localized overmelting due to steep thermal gradients.

In the case of 8-YSZ, the lower thermal conductivity resulted in shallower molten regions, though surface smoothness was maintained at moderate power levels (approximately 103–155 W). Continuous, crack-free coatings were obtained within this intermediate range, while incomplete sintering occurred at a lower power of 94 W. Conversely, excessive power exceeding 163 W caused undesirable substrate penetration.

SiC coatings exhibited larger molten areas owing to their high thermal conductivity. Moderate power levels (approximately 155–179 W) yielded continuous and smooth sintered layers. Inadequate sintering was observed at 147 W, whereas excessive power (187 W or higher) triggered substrate melting.

Laser power critically affected coating morphology and quality. Proper energy control balanced densification and surface integrity, providing a basis for subsequent microstructural and mechanical analyses. Representative OM and SEM images are presented in Fig. 1.

3.2 X-ray diffraction analysis after laser sintering

The phase structures of the laser-sintered ceramic coatings were analyzed by XRD, as shown in Fig. 2. The results indicate that the primary crystalline phases of all coatings were preserved after laser sintering.

For Al_2O_3 coatings [Fig. 2(a)], diffraction peaks at $2\theta \approx 35$, 43, and 57° were consistent with those of the original powder, indicating that no significant phase transformation occurred despite localized high-temperature exposure. This confirms the good thermal stability of Al_2O_3 during laser processing.

The XRD patterns of 8-YSZ coatings [Fig. 2(b)] exhibited characteristic peaks at $2\theta \approx 30$, 50, and 60°, corresponding to the stable cubic phase. Rapid heating and cooling during laser sintering effectively suppressed phase transformation, maintaining phase stability.

For SiC coatings [Fig. 2(c)], the prominent diffraction peaks at $2\theta \approx 35.6$, 41.4, and 60° showed no apparent shift after laser processing, indicating that crystallinity was preserved. Although minor oxidation may occur under high-power conditions, the overall phase stability remained intact.

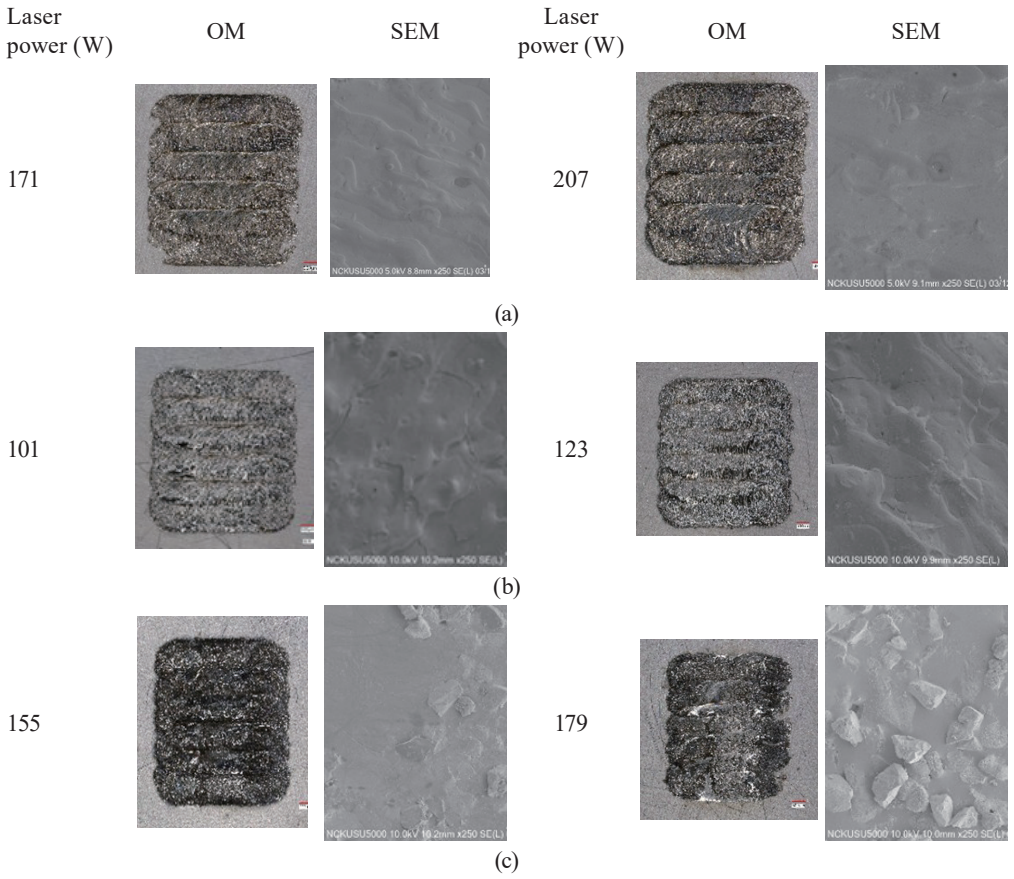

Fig. 1. OM and SEM images of laser-sintered (a) Al_2O_3, (b) 8-YSZ, and (c) SiC coatings prepared under different laser power conditions, showing variations in melting behavior and surface morphology.

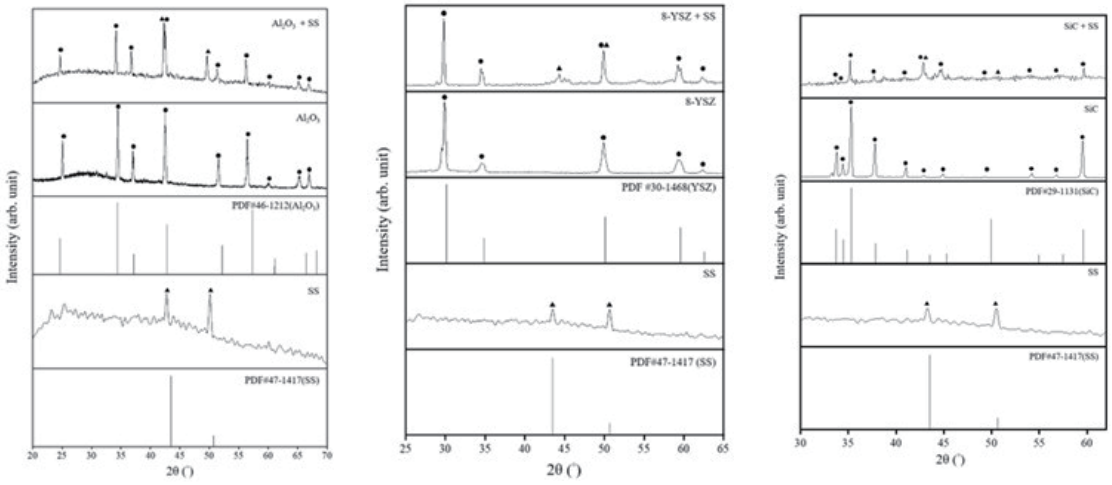

Fig. 2. XRD patterns of laser-sintered (a) Al_2O_3, (b) 8-YSZ, and (c) SiC coatings demonstrate preserved crystalline phases after laser processing.

The results of XRD analysis confirm that laser sintering enables the rapid, high-energy-density consolidation of ceramic coatings while maintaining phase stability. The observed fluctuations in diffraction peak intensities are primarily attributed to texture effects and changes in coating densification rather than phase decomposition. The rapid heating and cooling cycles inherent in laser processing can induce preferred crystallographic orientations during solidification, leading to the increase or reduction in specific peak intensity. This structural stability provides a reliable basis for subsequent mechanical and thermal performance analyses.

3.3 Vickers hardness analysis after laser sintering

Vickers hardness measurements were performed to evaluate the effects of laser power and material properties on the mechanical strength of the laser-sintered ceramic coatings. Tests were conducted under a load of 9.81 N with a dwell time of 20 s. For clarity, the hardness values are given in N/mm^2 (where 1 N/mm^2 = 1 MPa), and the conversion to conventional Vickers units (HV) can be performed using the relationship 1 HV ≈ 9.807 N/mm^2.[24] Five indentations were measured for each specimen, and the average was reported. All measurements were taken at the central region of the coatings to minimize edge effects.

For Al_2O_3 coatings, hardness increased with medium-to-high laser power levels (approximately 171–207 W), reaching a maximum of about 2780 N/mm^2 (283 HV), as shown in Fig. 3(a). This trend is attributed to enhanced melting and densification, which reduced porosity and crack density, as also observed in cross-sectional SEM images.

For 8-YSZ coatings, the maximum hardness was approximately 2780 N/mm^2 (283.5 HV), with a slight increase as laser power increased [Fig. 3(b)]. The low thermal conductivity and high phase stability of 8-YSZ facilitated the formation of fine-grained structures during rapid cooling. The highest hardness was obtained at 155 W, while excessive power resulted in minor porosity and thermal cracking, leading to a slight reduction in hardness.

SiC coatings exhibited the highest hardness among the three materials, with a peak value of approximately 7560 N/mm^2 (771 HV) at 179 W [Fig. 3(c)]. At low power, incomplete melting led to lower hardness, whereas optimal densification at around 179 W yielded the peak hardness. Further increases in power induced melt pool instability and thermal stress, reducing hardness.

Hardness increased with coating densification; however, excessive energy input eventually degraded the mechanical performance. In addition to porosity, the accumulation of residual thermal stresses and the development of microcracks play critical roles in the observed hardness trends, especially at the highest power level. The rapid cooling rates inherent in laser sintering induce significant thermal gradients, which can lead to localized thermal stresses and microscopic fissuring within the ceramic matrix. When the laser power exceeds the optimal threshold, these defects counteract the benefits of densification, thereby resulting in a slight reduction in measured Vickers hardness. These results confirm that the appropriate control of laser energy is essential for achieving a balance between high hardness and structural stability in ceramic coatings.

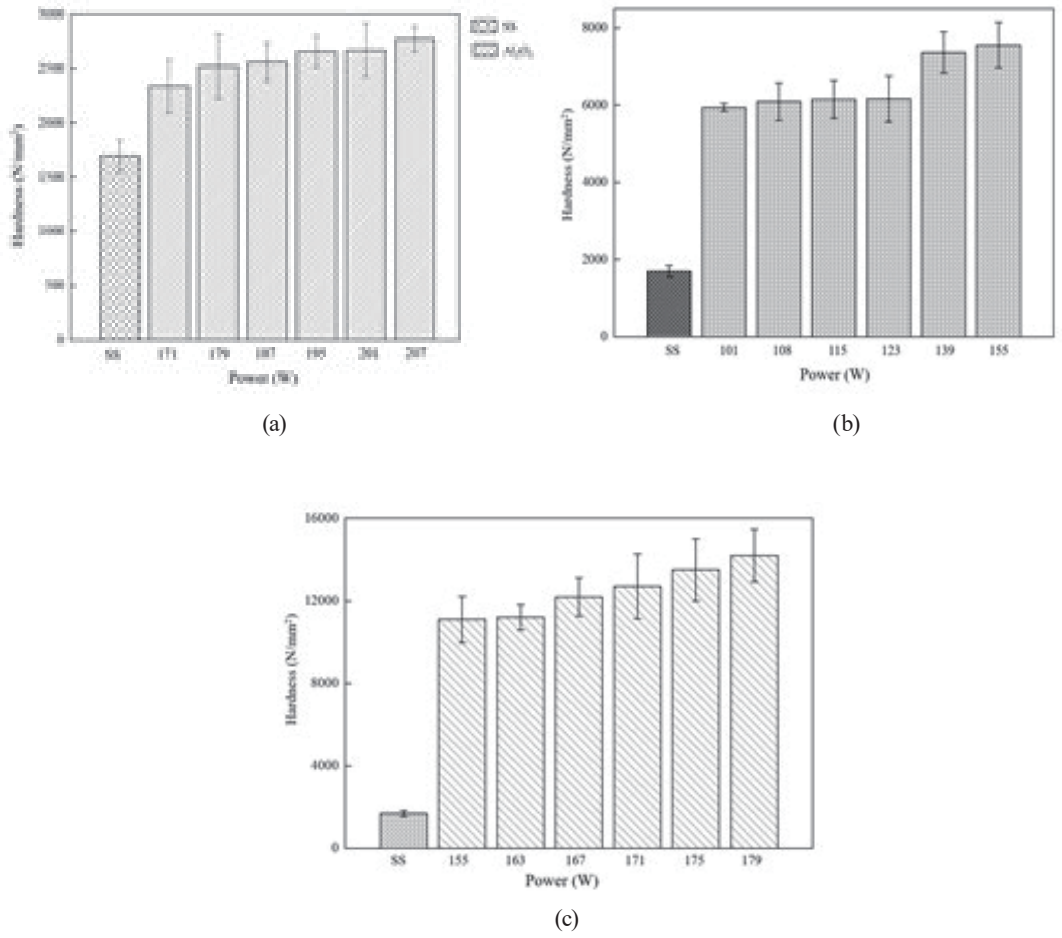

Fig. 3. Vickers hardness of laser-sintered (a) Al_2O_3, (b) 8-YSZ, and (c) SiC coatings as a function of laser power, showing the effects of energy input on coating densification and hardness.

3.4 Wear behavior after laser sintering

Wear tests were conducted on laser-sintered ceramic coatings to evaluate their tribological performance. The results indicate that the coatings significantly enhanced the wear resistance of the 304 stainless steel substrate through distinct mechanical interactions.

For Al_2O_3 coatings, the average friction coefficient stabilized between 0.42 and 0.46. The dominant wear mechanisms were identified as mild polishing and microcleavage. Initially, surface asperities and particle boundaries were leveled through polishing, leading to a stable sliding interface. Subsequently, the high hardness and intrinsic brittleness of Al_2O_3 resulted in localized microcleavage under cyclic loading, though the overall coating integrity remained high [Fig. 4(a)].

In the case of 8-YSZ coatings, the friction coefficient exhibited a downward trend over time. This behavior signifies a transition in the dominant mechanism from initial abrasive cutting to mild polishing. The wear tracks remained remarkably smooth and free of delamination,

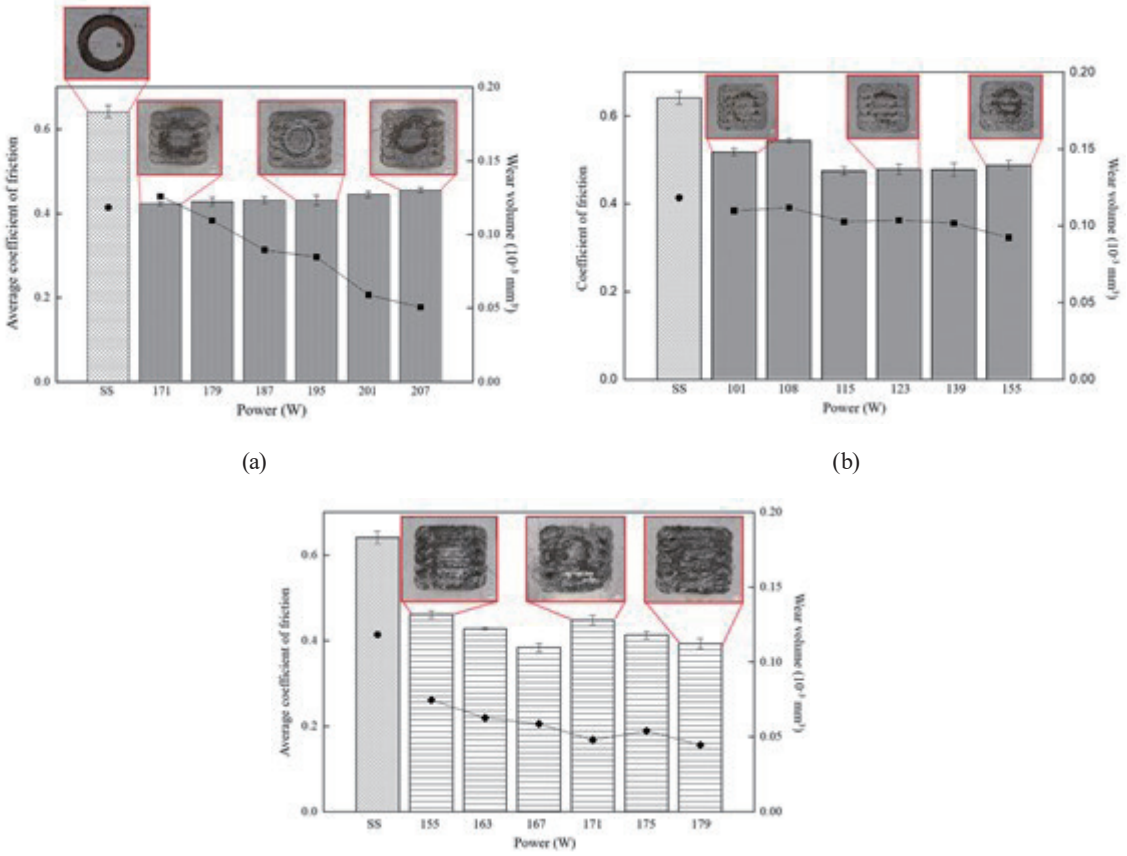

Fig. 4. (Color online) Wear track morphologies of laser-sintered ceramic coatings, (a) Al_2O_3, (b) 8-YSZ, and (c) SiC, showing representative surface conditions after sliding tests.

demonstrating superior shear resistance and the ability of 8-YSZ to maintain stable contact conditions [Fig. 4(b)].

SiC coatings exhibited the lowest friction coefficients (approximately 0.38–0.42) and a 60% reduction in wear rate compared with the 304 stainless steel substrate. The wear behavior was primarily governed by an abrasive wear mechanism, complemented by minor plastic deformation. The optimal densification achieved at 179 W significantly bolstered the coating's resistance to abrasive grooving. As shown in Fig. 4(c), the SiC surfaces exhibited minimal damage, confirming its superior structural stability in high-friction environments.

Overall, SiC demonstrated the highest wear resistance among the three coatings, followed by Al_2O_3 and 8-YSZ, confirming that laser sintering effectively optimizes the tribological performance of ceramic-based surface reinforcements.

4. Conclusions

Al_2O_3, 8-YSZ, and SiC ceramic coatings were successfully fabricated on 304 stainless steel substrates via laser sintering. The effects of laser energy input on coating microstructure, phase

stability, hardness, and wear behavior were systematically evaluated. The results indicated that laser sintering enables rapid, localized high-temperature processing while maintaining good coating integrity.

X-ray diffraction analysis confirmed that all coatings retained their primary crystalline phases after laser sintering, indicating the effective suppression of phase transformation during rapid heating and cooling. Microscopic observations showed that an appropriate laser power enhanced coating densification and surface continuity, whereas insufficient or excessive energy led to incomplete sintering or localized overmelting.

Vickers hardness measurements revealed a clear dependence on coating densification. Al_2O_3 and 8-YSZ coatings achieved maximum hardness values of approximately 2780 N/mm² under optimal conditions, while SiC coatings exhibited the highest hardness, reaching approximately 7560 N/mm². Excessive energy input caused defect formation and a slight reduction in hardness.

Wear tests demonstrated that laser-sintered ceramic coatings showed significantly improved tribological performance compared with the stainless steel substrate. Al_2O_3 and 8-YSZ coatings showed stable friction behavior, while SiC coatings exhibited the lowest friction coefficient and the most significant wear resistance. These findings confirmed that the precise control of laser energy is critical for optimizing coating performance and highlighted laser sintering as a practical approach for high-wear applications.

Acknowledgments

This work was supported by the National Science and Technology Council (NSTC), Taiwan, under Grants No. 112-2221-E-006-173, 113-2221-E-006-087-MY2, 113-2221-E-006-112-MY2, and 113-2221-E-006-116. The authors gratefully acknowledge the Core Facility Center at National Cheng Kung University, Taiwan, for providing access to the EM000800 and SQUID000200 instruments, which were funded by the NSTC project 114-2740-M-006-001. Additional support from the Higher Education Sprout Project of the Ministry of Education, Taiwan, through the Headquarters of University Advancement at National Cheng Kung University (NCKU), is also gratefully acknowledged.

References

1 S.-C. Shi, Y.-C. Xu, C.-K. Chen, and B.-T. Ko: Sens. Mater. **37** (2025) 1808. https://doi.org/10.18494/SAM5312
2 S.-C. Shi, T.-H. Chen, and P. K. Mandal: Polymers **12** (2020) 1246. https://doi.org/10.3390/polym12061246
3 D. Rahmadiawan and S.-C. Shi: Scientific Reports **14** (2024) 9217. https://doi.org/10.1038/s41598-024-59010-w
4 D. Chen, H. Zhang, G. Zhao, Z. Zhu, J. Yang, J. He, J. Li, Z. Yu, and Z. Zhu: Langmuir **40** (2024) 12322. https://doi.org/10.1021/acs.langmuir.4c01805
5 K. He, Y. Chen, H. Lai, and X. Wu: J. Constructional Steel Res. **224** (2025) 109144. https://doi.org/10.1016/j.jcsr.2024.109144
6 P. Shao, J. Ren, X. Wang, X. Zou, C. Ying, G. Dou, Y. Jin, M. Yu, B. Yang, and M. Yuan: J. Phys. Conf. Ser. **3112** (2025) 012069. https://doi.org/10.1088/1742-6596/3112/1/012069
7 Z. Yu, Z. Liu, F. Ye, C. Ramadini, and L. Xia: Corros. Sci. **197** (2022) 110098. https://doi.org/10.1016/j.corsci.2022.110098
8 A. Meghwal, A. Anupam, V. Luzin, C. Schulz, C. Hall, B. Murty, R. S. Kottada, C. C. Berndt, and A. S. M. Ang: J. Alloys Compd. **854** (2021) 157140. https://doi.org/10.1016/j.jallcom.2020.157140
9 J. Kitamura, H. Mizuno, N. Kato, and I. Aoki: Mate. Trans. **47** (2006) 1677. https://doi.org/10.2320/matertrans.47.1677

10 S. H. Park, K. E. Kim, and S. J. Hong: Coatings **11** (2021) 105. https://doi.org/10.3390/coatings11010105
11 Y. Liu, M. Wu, Z. Zhang, Y. Wang, L. Meng, K. Cai, H. Zhu, K. Xu, and J. Lu: J. Mater. Process. Technol. **326** (2024) 118340. https://doi.org/10.1016/j.jmatprotec.2024.118340
12 D. Bartkowski, A. Bartkowska, and P. Jurči: Opt. Laser Technol. **136** (2021) 106784. https://doi.org/10.1016/j.optlastec.2020.106784
13 P. Xu, C. Lin, C. Zhou, and X. Yi: Surf. Coat. Technol. **238** (2014) 9. https://doi.org/10.1016/j.surfcoat.2013.10.028
14 O. Ertugrul, T. M. Enrici, H. Paydas, E. Saggionetto, F. Boschini, and A. Mertens: Powder Technol. **375** (2020) 384. https://doi.org/10.1016/j.powtec.2020.07.100
15 R. L. Winter, P. Singh, M. K. King Jr, M. K. Mahapatra, and U. Sampathkumaran: Adv. Mater. Sci. Eng. **2018** (2018) 9121462. https://doi.org/10.1155/2018/9121462
16 M. Ramesh, K. Marimuthu, P. Karuppuswamy, and L. Rajeshkumar: Boletín de la Sociedad Española de Cerámica y Vidrio **61** (2022) 641. http://doi.org/10.1016/j.bsecv.2021.06.004
17 M. T. Mehran, R.-H. Song, T.-H. Lim, S.-B. Lee, J.-W. Lee, and S.-J. Park: Mater. Energy, Effic. Sustainability TechConnect Briefs **2** (2016) 98.
18 A. R. Hanifi, M. A. Laguna-Bercero, N. K. Sandhu, T. H. Etsell, and P. Sarkar: Sci. Rep. **6** (2016) 27359. https://doi.org/10.1038/srep27359
19 A. H. Raza, S. Farhan, A. Ali, A. Sarfraz, M. A. Ahmad, M. Syväjärvi, and R. Raza: J. Solid State Electrochem. **29** (2025) 1777. https://doi.org/10.1007/s10008-024-06128-6
20 Y. Wang, L. Gao, L. Yang, T. Liu, J. Miao, Y. Zang, and S. Zhang: Appl. Sci. **14** (2024) 9686 https://doi.org/10.3390/app14219686
21 W. Xie, H.-C. Man, and C.-W. Chan: J. Magnesium Alloys **12** (2024) 1346. https://doi.org/10.1016/j.jma.2023.11.005
22 Z. Gao, L. Wang, Y. Wang, F. Lyu, and X. Zhan: J. Alloys Compd. **903** (2022) 163905. https://doi.org/10.1016/j.jallcom.2022.163905
23 H. Maurya, K. Kosiba, K. Juhani, F. Sergejev, and K. Prashanth: Addit. Manuf. **58** (2022) 103013. https://doi.org/10.1016/j.addma.2022.103013
24 S. A. Shahdad, J. F. McCabe, S. Bull, S. Rusby, and R. W. Wassell: Dent. Mater. **23** (2007) 1079. https://doi.org/10.1016/j.dental.2006.10.001